ICAS PAPER NO. 72 – 25

EXPERIMENTAL INVESTIGATIONS OF SEPARATED
FLOWS ON WING-BODY COMBINATIONS
WITH VERY SLENDER WINGS
AT MACH NUMBERS M = 0.5 to 2.2

by
W. Stahl, K. Hartmann and
W. Schneider, Research Engineers
DFVLR, Aerodynamische Versuchsanstalt
Göttingen, Germany

The Eighth Congress of the International Council of the Aeronautical Sciences

INTERNATIONAAL CONGRESCENTRUM RAI-AMSTERDAM, THE NETHERLANDS
AUGUST 28 TO SEPTEMBER 2, 1972

Price: 3. Dfl.

EXPERIMENTAL INVESTIGATIONS OF SEPARATED FLOWS ON WING-BODY COMBINATIONS WITH VERY SLENDER WINGS AT MACH NUMBERS $M_\infty = 0.5$ TO 2.2

W. Stahl, K. Hartmann and W. Schneider

Dr.-Ing., Dipl.-Ing., Dipl.-Ing.

DEUTSCHE FORSCHUNGS- UND VERSUCHSANSTALT
FÜR LUFT- UND RAUMFAHRT E. V.
- Aerodynamische Versuchsanstalt Göttingen -

Göttingen, Federal Republic of Germany

Abstract

An investigation has been undertaken, in order to find out, to what extent the flow field of a slender delta wing with its favourable properties would be carried over to a wing-body combination. Such a flow is governed by the leading edge vortices, and it does not change essentially over a wide range of Mach numbers and angles of attack. A wing-body combination with a very slender wing (A = 0.52) extending along most of the body, was tested to this end. Forces and pressure distributions on suction and pressure sides were obtained at subsonic, transonic and supersonic flow velocities ($0.5 \leq M_\infty \leq 2.2$) for angles of attack up to $\alpha \approx 30^\circ$. The Reynolds number was held constant for all Mach numbers at $R = 2.7 \cdot 10^6$ (based on two third of the wing length). Oil and smoke flow visualization techniques gave some insight into the flow structure.

Notations

A	wing aspect ratio, $A = \frac{b^2}{S}$
b	wing span at trailing edge
c_p	pressure coefficient, $c_p = \frac{p - p_\infty}{q_\infty}$
c_Z	normal force coefficient, $c_Z = \frac{Z}{q_\infty S}$
D	body diameter
l	length of wing
L	length of body
M_∞	free-stream Mach number
p	static pressure
p_∞	free-stream static pressure
q_∞	free-stream dynamic pressure, $q_\infty = \frac{1}{2} \rho_\infty U_\infty^2$
R, R_D	Reynolds number, $R = \frac{U_\infty \cdot 2/3\,l}{\nu_\infty}$; $R_D = \frac{U_\infty \cdot D}{\nu_\infty}$
s	wing semi span
S	wing plan-form area
U_∞	free-stream velocity
x, y, z	coordinate system fixed in the wing
Δx_{cp}	distance of center of pressure from center of area of wing, positive downstream
Z	normal force
α	angle of attack
ν_∞	free-stream kinematic viscosity of air
ρ_∞	free-stream density of air

I. Introduction

Interest has long been existing in the slender delta wing, as its flow field has beneficial properties. This flow field, which is strongly influenced by the leading edge vortices, maintains its pertinent features from low speeds into the supersonic regime, as long as the edges are swept back well behind the Mach cone. Also, we have the same basic flow up to large angles of attack, the upper limit being set by vortex break-down, occurring above the wing. The slender delta wing, with its essentially conical flow, has the resultant force acting in or near the center of area in a wide range of flying conditions. These favourable properties have been deliberately exploited for the supersonic transport in the past [1]. As a next step, it seemed worth-while trying to make use of them for other applications, e. g. for missile-like configurations.

The work, reported on here, was undertaken within the framework of a collaboration in aerodynamics, existing between DFVLR and Royal Aircraft Establishment.

II. Wind Tunnel, Measuring Equipment, and Models

The Transonic Wind Tunnel of the Aerodynamische Versuchsanstalt Göttingen, which was used for the force and pressure measurements, is a closed circuit, continuously operating tunnel for Mach numbers from $M_\infty = 0.4$ to $M_\infty = 2.2$. For measurements in supersonic flow, $M_\infty > 1.2$, the model is situated in the test section of the Laval nozzle; at subsonic and transonic speeds, $M_\infty = 0.4 - 1.2$, the transonic test section is used. It has perforated walls with inclined holes, the porosity being 6 %. Suction from this test section is applied at Mach numbers $M_\infty > 0.9$. The cross-section of both test sections is 1 m x 1 m. The total pressure can be varied between 0.25 at and 2.0 at; the total temperature is about 50° C. The tunnel is described in detail in [2] and [3].

Normal forces and pitching moments were measured with a strain gauge balance.

The wing-body combination consists of a very slender delta wing (with an aspect ratio of A = 0.52) and of a cylindrical body, having an ogival nose.

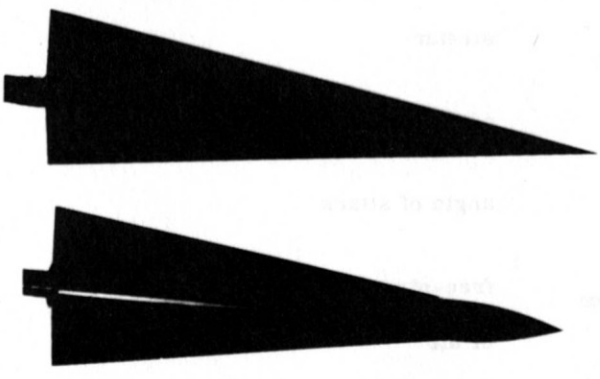

Figure 1. Delta wing and wing-body combination

The model is shown in Fig. 1, also the wing alone. The body diameter is D = 40 mm; the length of the body is L = 520 mm ≈ 13 D, inclusive of the nose of 3 diameter length. The delta wing has a length of l = 540 mm = 13.5 D; the trailing edge span is b = 139 mm ≈ 3.5 D. The exposed wings extend from the body's base along the body for 9.6 D. One model has built in such a way, that the exposed wings were directly suspended in strain gauge balances in the body. The pressure taps on the wing lie on straight lines passing through the wing apex, on the body they lie on straight lines parallel to the axis. Further details and the principal dimensions are given in Fig. 2.

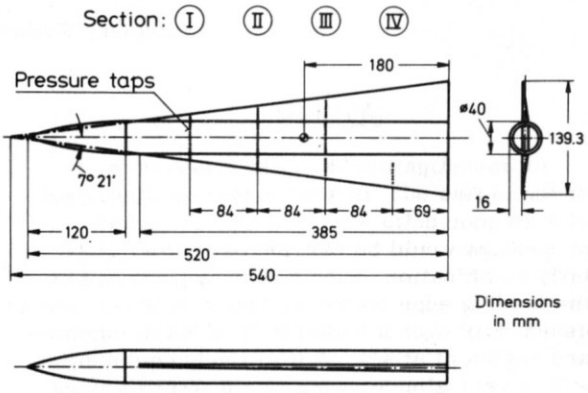

Figure 2. Views and principal dimensions of models

For some of the smoke flow visualization experiments, a flat plate delta wing of aspect ratio A = 1 was used. The smoke flow studies, as well as the oil flow pictures, were made in the intermittently working High- Speed Wind Tunnel of AVA, with a test section of 0.75 m x 0.75 m. It is operating in the Mach number ranges $0.40 \leq M_\infty \leq 0.94$ and $1.22 \leq M_\infty \leq 2.50$.

The classical smoke flow visualization technique was further developed at AVA for use at high flow velocities; it is fully described in [4].

III. Test Program

The test program comprised normal force, pitching moment and pressure measurements; the latter were made in four sections on suction and pressure sides. Free-stream Mach numbers were:

M_∞ = 0.50, 0.70, 0.80, 0.90, 0.95, 1.00, 1.10, 1.20, 1.46, 1.79, and 2.21.

The range of angles of attack was:

$$0^\circ \lesssim \alpha \lesssim 30^\circ;$$

the Reynolds number was held constant for all Mach numbers:

$$R = \frac{U_\infty \cdot (2/3)\, l}{\nu_\infty} = 2.7 \cdot 10^6 ,$$

or, based on the body diameter:

$$R_D = \frac{U_\infty \cdot D}{\nu_\infty} = 3 \cdot 10^5 .$$

IV. Results and Discussion

a) Forces and pressure distributions

At first some results are presented of the force measurements on the wing-body combination, the wing alone, and on the exposed wings in presence of the body, performed at high subsonic, transonic, and supersonic flow velocities, for constant Reynolds number

$$R = \frac{U_\infty \cdot (2/3)\, l}{\nu_\infty} = 2.7 \cdot 10^6 .$$

In Fig. 3 the normal force coefficient is given as a function of angle of attack for the wing-body combination.

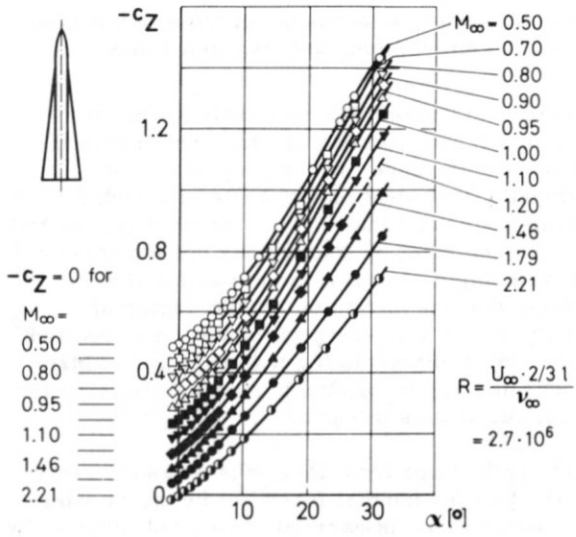

Figure 3. Normal force coefficient versus angle of attack for wing-body combination

The distinctly non-linear behaviour of the normal forces with incidence is essentially equivalent to what has been obtained for the slender wing alone in earlier tests by the authors [5]. From this, one draws immediately the conclusion, that leading edge vortices are present as strongly as on the wing alone. These leading edge vortices are responsible for the overriding part of the non-linear component of the normal force, the contribution of vortices possibly developing on the short forebody, is likely to be small. Some evidence is provided for this statement by oil flow pictures. In order to obtain some insight into the flow on the suction sides of the wing and the wing-body combination, two smoke flow visualization pictures are given for a transonic Mach number (Fig. 14). There, one can clearly see the leading edge vortices, being illuminated in a light plane perpendicular to the model; the upper picture shows the wing alone, in the lower one, we have the wing-body combination with the vortex flow displaced outward (about 10 % of local semi span), due to the effect of the body.

Besides determining the normal forces acting on the wing alone and on the wing-body combination, we have also measured the normal forces experienced by the exposed wings in presence of the body, by mounting them on balances within the body. These results enable us to judge the effect on the normal force of adding the body to the wing, as well as to evaluate the distribution of the normal force, acting on the individual components, i. e., on the exposed wings and on the body. In Fig. 4 the normal force coefficient is plotted versus the free stream Mach number for a small, a moderate and a large angle of attack.

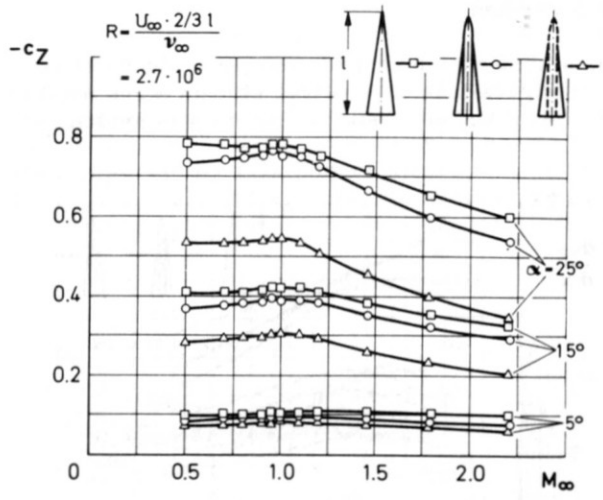

Figure 4. Normal force coefficient of wing, wing-body combination and exposed wings

The wing-body combination experiences a distinctly diminished normal force, as compared with the wing alone, the difference being a minimum in the transonic regime. This influence of adding a body to the wing is in qualitative accordance with

the predictions of slender-body theory, though this theory is based on a flow, which remains attached around the leading edges, in contrast to what we have. The variation with Mach number of the measured results, is not given by this theory.

Comparison of the results obtained from the complete wing-body combination and from the exposed wings in that combination, shows, that a large proportion of the normal force is carried by the exposed wings, namely 70 - 80 % of the force acting on the wing-body combination, and this is to be seen valid throughout the whole Mach number range investigated, with a tendency of the wing's contribution to decrease with increasing incidence. It is to be added, that the projected areas are of about the same size for the exposed wings and for the body. These findings should be further substantiated, of course, by the results of the pressure measurements, which were performed in several spanwise sections on suction and pressure sides, and which will be discussed later on.

Examining the non-linear behaviour of slender wing-body combinations, it is necessary to estimate the influence of the components, as the wing alone, the body alone and the interference effects between these components, when combined to the full combination. In this paper, it is only possible to touch such questions. A more detailed description of these problems, in particular interference effects, can be found in [6]. Here, only the dependance on Mach number and angle of attack of the normal force curve slope and the position of the center of pressure are described.

Fig. 5 shows the normal force curve slopes of all the configurations versus free stream Mach number at constant angles of attack. Here, it is evident,

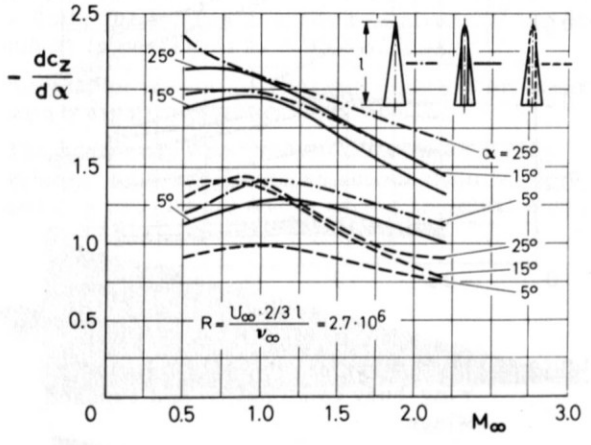

Figure 5. Slope of normal force coefficient curve

that there is a dependance on Mach number, especially at supersonic speeds. For the wing and the wing-body combination the non-linearity in normal force, caused by the strong leading edge vortices, appears below an incidence of $\alpha \approx 15^o$. At higher incidence, the non-linearity ceases. For the exposed wings, it occurs only below $\alpha \approx 10^o$, at higher incidence the normal force curve's slope becomes nearly constant.

Some influence of compressibility on the position of center of pressure is seen for the wing, the wing-body combination and the exposed wings at subsonic speeds in Fig. 6 .

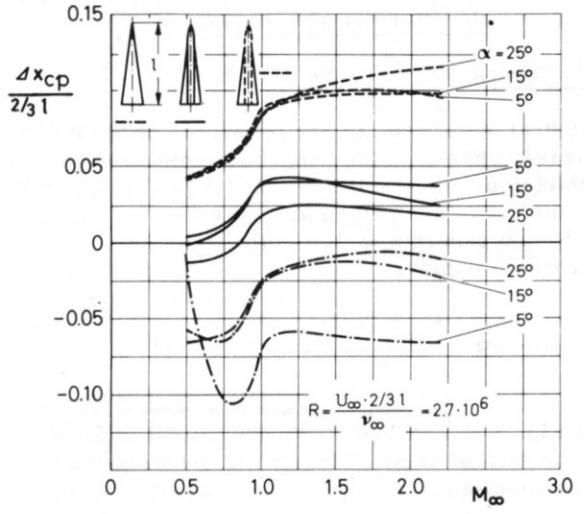

Figure 6. Center of pressure of wing, wing-body combination, and exposed wings

The center of pressure moves downstream for nearly 0. 5 D with increasing Mach number in the subsonic speed range. While its position is additionally dependent on the angle of attack for the wing-body combination and, especially, for the wing, the center of pressure does not move very much with angle of attack for the exposed wings. The fact, that the movement of the center of pressure on the wing-body combination is limited to about half a diameter for a wide range of Mach numbers and angles of attack seems promising for its application as a missile.

The above findings from the force measurements, namely, that the normal force acting on the wing-body combination, is carried, to a great extent, by the exposed wings, at all angles of attack and at all Mach numbers investigated, will now be followed up by means of the measured spanwise pressure distributions in various sections. The results presented here, are restricted to examples at one subsonic, transonic, and supersonic Mach number, the complete results are given in [7] .

Fig. 7 contains the pressure distributions on the suction side of the combination at M = 0.7 . At the lower angle of incidence, $\alpha = 10^{o}$, the suction on most part of the body is comparatively small, with a suction peak at the side, full suction being developed only on the wing.

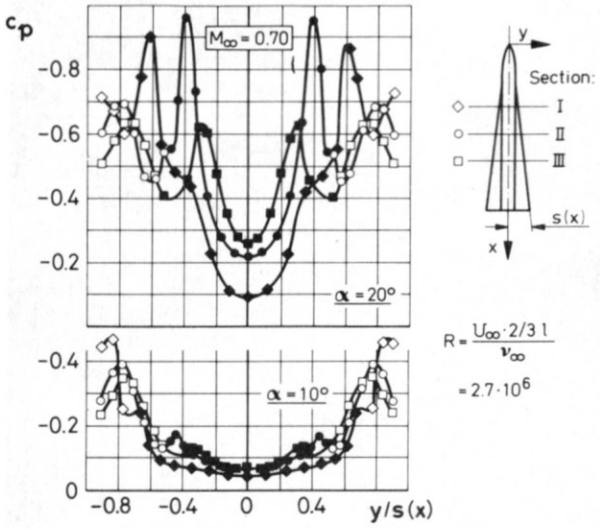

Figure 7. Spanwise pressure distributions of wing-body combination (suction side)

As the leading edge vortex lifts off the surface of the wing and moves somewhat inboard downstream, the suction peaks both on the body and on the wing decrease. The information obtained from the pressure distributions, is in good agreement with the interpretations of the oil flow pictures, discussed below.

The pressures at transonic flow velocity have qualitatively the same spanwise distribution, but the overall level has decreased notably, see Fig. 8.

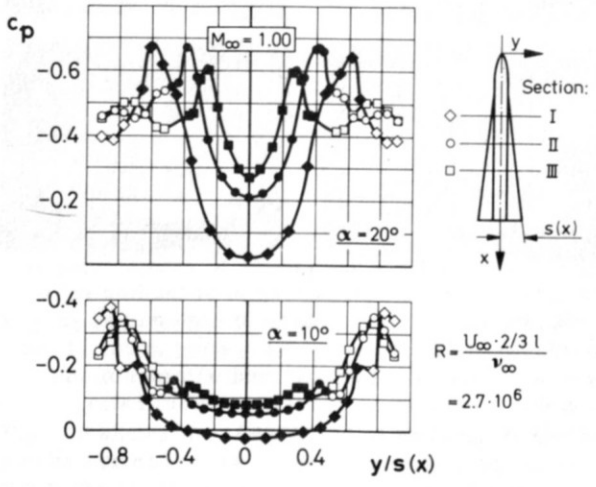

Figure 8 . Spanwise pressure distributions of wing-body combination (suction side)

This loss in load on the suction side of the wing-body combination with increasing Mach number has already been observed for the wing alone. The pressure distribution preserves its basic features also at the supersonic Mach number, Fig. 9. except for the fact, that a third suction peak can be observed at the foremost section I.

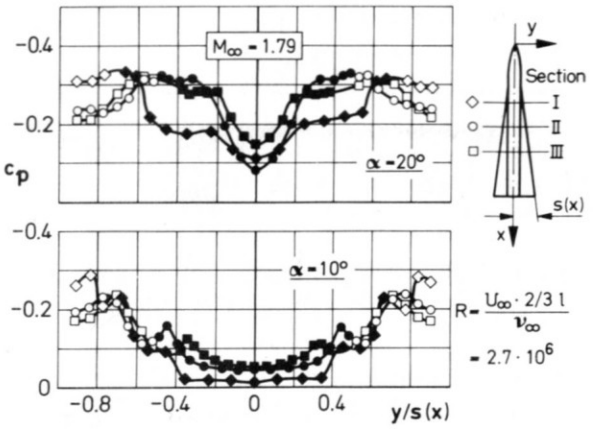

Figure 9. Spanwise pressure distributions of wing-body combination (suction side)

The loss in load continues, with the Mach number having been increased further into the supersonic regime, the decreased suction being felt more by the wing than by the body. Examining the pressure distributions at the larger angle of attack, $\alpha = 20^{o}$, at subsonic and transonic velocities, we observe, that the suction peaks on the body and on the wing are now of about the same strength (section III). This is in agreement with the fact, that the leading edge vortex has about the same distance from the body and from the wing, respectively, as can be seen in the smoke flow picture already mentioned above (Fig. 14). In the middle section (II) the peak is even higher on the side of the body than it is on the wing.

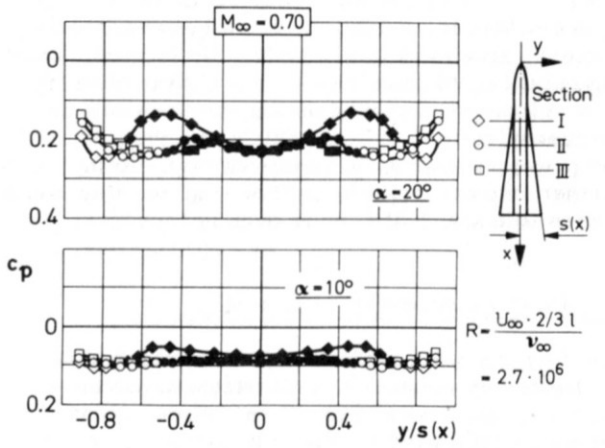

Figure 10. Spanwise pressure distributions of wing-body combination (pressure side)

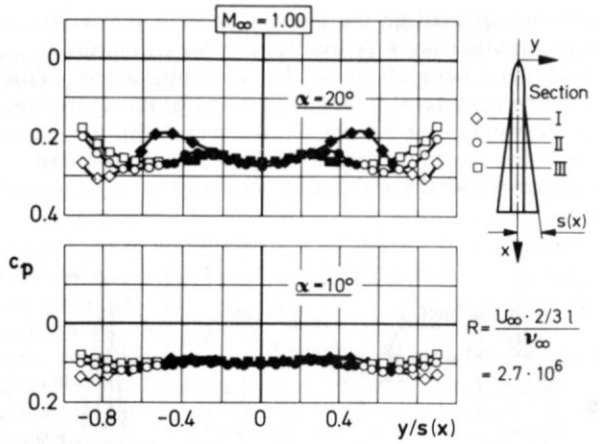

Figure 11. Spanwise pressure distributions of wing-body combination (pressure side)

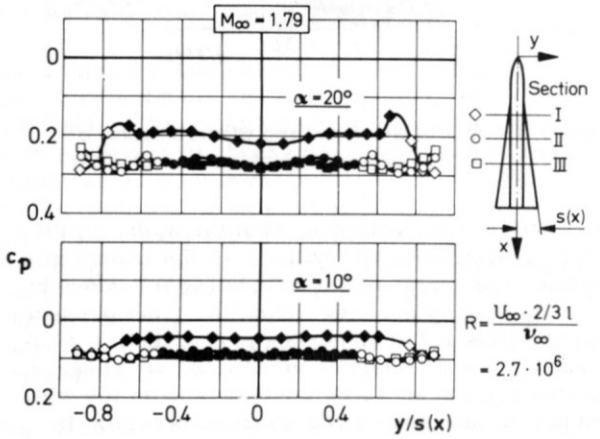

Figure 12. Spanwise pressure distributions of wing-body combination (pressure side)

We turn now to the pressure distributions on the pressure side of the wing-body combination, again at one subsonic, transonic, and supersonic Mach number, given in Fig. 10 to 12. Here, the interesting point is, that the loss in load with increasing flow velocities observed on the suction side, is compensated for, to some extent, by the gain on the pressure side up to sonic velocity. Going further into the supersonic flow regime, this trend comes to a stand-still or is even reversed.

b) Flow visualization

The flow near the surface of the models was investigated by means of an oil titanium-oxyde mixture, which was sprayed on the model and exposed to the wind for some seconds. These flow pictures permit also some insight into the general flow field. Fig. 13 shows an example at $M_\infty = 0.9$.

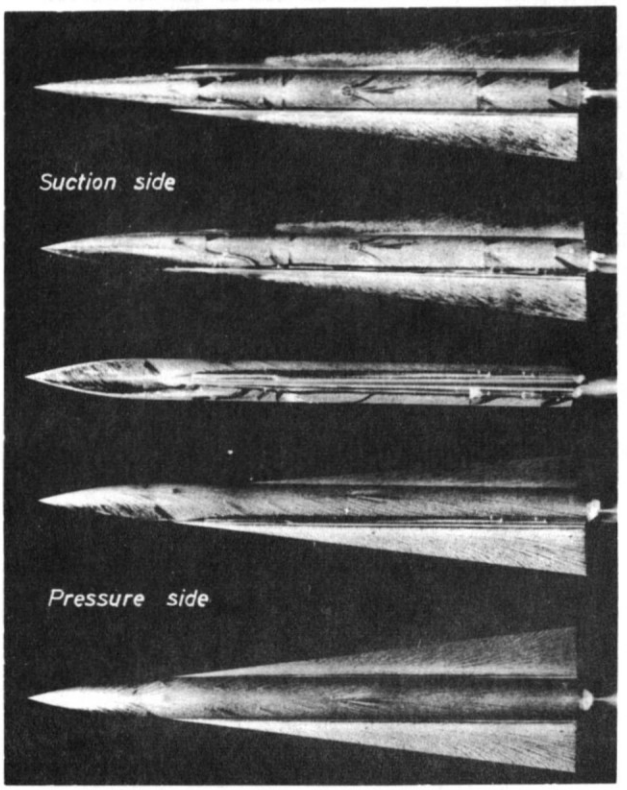

Figure 13. Oil flow pictures from suction and pressure sides of wing-body combination, M = 0.9, $\alpha = 20^\circ$

On the suction side one has the typical pattern of a flow with leading edge vortices, and, at least on the rear part of the wing, the flow separates near the leading edge in the pressure field of the vortex (secondary separation). At the junction of wing and body, there are other separation regions to be observed, on the suction side as well as on the pressure side.

Smoke flow visualization on the wing alone and on the wing-body combination, in planes normal to the models, gives a good impression of the leading edge vortices (Fig. 14). The flow about the wing-body combination is nearly as much dominated by the vortices, as is the case for the wing alone.

Also, attempts have been made to obtain some information about the phenomenon of leading edge vortex bursting, taking place at high angles of attack. In order to have the bursting occur at incidences, which could be attained with our model support, a delta wing of larger aspect ratio, namely A = 1, had to be chosen.

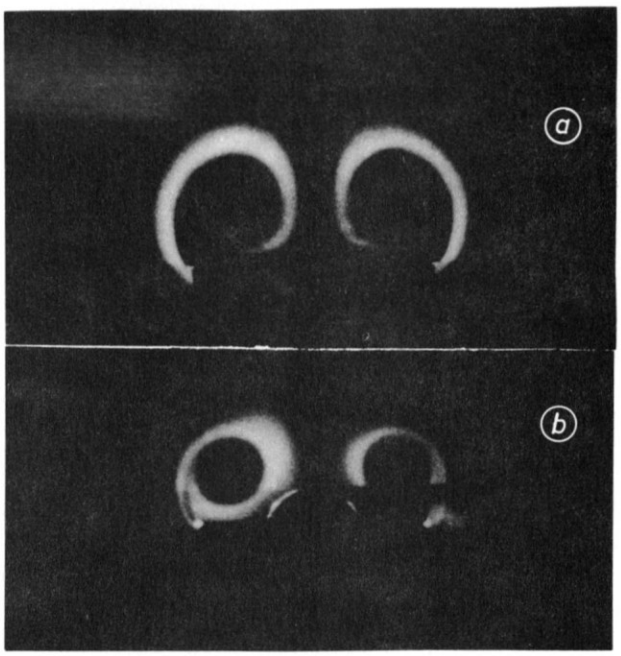

Figure 14. Smoke flow visualization in a plane normal to the model (section III)
$M_\infty = 0.9$; $\alpha = 20^o$
(a) Wing (b) Wing-body combination

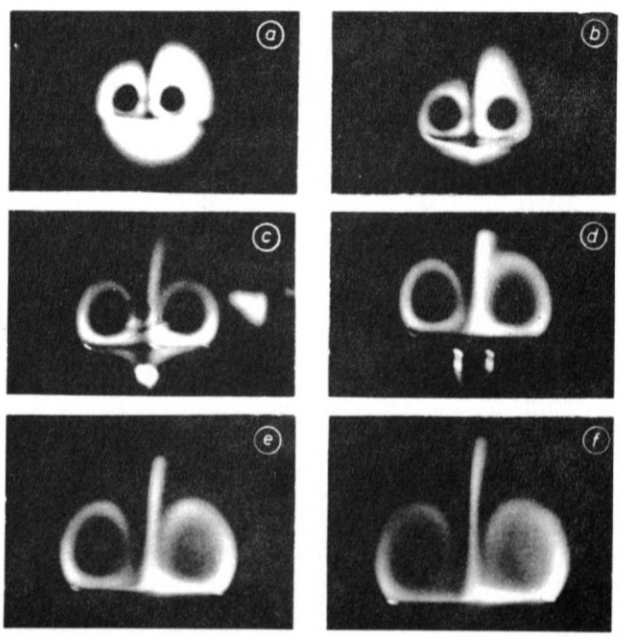

Figure 15. Smoke flow visualization of vortex bursting on slender delta wing (A = 1)
$M_\infty = 0.6$; $\alpha \approx 38^o$

Fig. 15 shows the leading edge vortex again in planes normal to the model at different sections, the angle of attack being $\alpha \approx 38^o$ and the free-stream Mach number $M_\infty = 0.6$. Observations of the wing in side views showed, that sections a and b were ahead of the beginning of the break down region, section c nearly at the beginning, sections d and e inside the break down region, and f at the end of it. One notices a change in the circular shape of the vortices to an oval one after the bursting has set in, and the presence of smoke inside the vortices. A more detailed investigation of these phenomena is planned.

V. Conclusions

The results of force measurements, undertaken on a wing-body combination with a very slender wing, on the exposed wings, and on the wing alone in subsonic, transonic, and supersonic flow have been reported. The normal force coefficient of the wing-body combination displays, at all flow speeds, the typical non-linear behaviour with angle of attack, due to the strong leading edge vortices of the slender wing; the non-linear part of the normal force being considerable. It experiences a distinctly diminished normal force at all incidences, as compared to the wing alone. The movement of the center of pressure is restricted to about half a body diameter, within a wide range of incidences in the whole Mach number range.

The spanwise pressure distributions on the suction side of the wing-body combination exhibit clearly the influence of the wing's leading edge vortices. In subsonic and transonic flow, a loss in load with increasing Mach number on the suction side, is compensated for, to some extent, by a gain on the pressure side.

Oil and smoke flow visualization techniques allow some insight into the flow patterns. The influental role of the leading edge vortices can be deduced from smoke pictures in planes normal to the models, and some information is obtained about vortex bursting.

VI. Acknowledgements

The authors wish to thank their colleagues of the Royal Aircraft Establishment at Farnborough and Bedford for many useful discussions and suggestions, especially Dr. D. Küchemann, Mr. G. G. Brebner, Mr. J. B. Ogle, and Mr. J. H. B. Smith. We are indebted to Prof. T. Sarpkaya, guest from Naval Post-Graduate School, Monterey, California, for his great help, given in connection with flow visualization problems.

VII. Literature

(1) Küchemann, D., "Aircraft shapes and their aerodynamics for flight at supersonic speeds," Advances in Aeronautical Sciences, Vol. 3, Pergamon Press, Oxford (1961), pp. 221 - 252

(2) Ludwieg, H., Lorenz-Meyer, W., Schneider, W., "Der Transsonische Windkanal der Aerodynamischen Versuchsanstalt Göttingen," Jahrbuch der WGLR 1966, pp. 145 - 155

(3) Lorenz-Meyer, W., Hottner, Th., "Der Transsonische Windkanal der Aerodynamischen Versuchsanstalt Göttingen (II. Ausbaustufe)," Jahrbuch der DGLR 1968, pp. 235 - 244

(4) Stahl, W., "Zur Sichtbarmachung von Strömungen um schlanke Deltaflügel bei hohen Unterschallgeschwindigkeiten," DFVLR/AVA-Report 70 A 45 (1970)

(5) Stahl, W., Hartmann, K., Schneider, W., "Force and pressure measurements on a slender delta wing at transonic speeds and varying Reynolds numbers," AGARD-CP-83-71 (1971), pp. 9-1 to 9-12

(6) Schneider, W., Stahl, W., Hartmann, K., "Interference effects on a slender wing-body combination in compressible flow, "DFVLR/AVA-Report, to be published

(7) Stahl, W., Hartmann, K., Schneider, W., "Aerodynamische Untersuchungen an Flugkörpern mit Flügeln kleiner Streckung," Teil II: "Kraft- und Druckverteilungsmessungen, sowie Strömungsbeobachtungen an einer Flügel-Rumpf-Kombination in Unterschall-, transsonischer und Überschallströmung," DFVLR/AVA-Report 71 A 26 (1972)